

# Coupled Electron Pair Approximation Calculation of the Electric Dipole Moment of Atomic Yb

Angom Dilip Singh  
Physical Research Laboratory,  
Navarangpura, Ahmedabad-380 009.

Bhanu Pratap Das  
Non-Accelerator Particle Physics Group,  
Indian Institute of Astrophysics,  
Sarjapur Road, Koramangala,  
Bangalore-34

Debashis Mukherjee  
Department of Physical Chemistry,  
Indian Association for Cultivation of Science ,  
Calcutta-32

The existence of a finite electric dipole moment (EDM)  $d_a$  of the closed-shell atom Yb implies parity and time reversal violations involving the nuclear sector. An important effect which can contribute to the Yb EDM is the tensor-pseudotensor electron-nucleus interaction characterized by the coupling constant  $C_T$ . Within the Standard Model (SM) of particle physics  $C_T = 0$ , as this form of interaction is not allowed. If a finite  $d_a$  of Yb is observed in experiments, then an estimate of  $C_T$  can be obtained by combining with the theoretical calculations. A non-zero  $C_T$  implies physics beyond the standard model. In this paper we present the result of our *ab initio* calculation of the EDM Yb using different many-body methods.

## I. INTRODUCTION

Discrete symmetry violations in atoms are important phenomena to probe for physics beyond the Standard Model(SM) of the particle physics. The electric dipole moment(EDM) of an atom, which is a signature of the simultaneous parity and time-reversal (P-T) symmetry violations is one such. There are several possible sources of P-T violation effects within an atom, the tensor pseudo-tensor electron nucleus interaction is an example which is semi-leptonic in nature. The atomic Yb, which is a closed-shell atom having a  $Z = 70$  is a very good candidate for atomic EDM experiments to probe for the nuclear sector effects. An additional advantage of using a rare Earth atom like Yb is the closely spaced energy levels. The experimental results when compared with the theoretical results can yield signatures of physics beyond the SM.

Among the closed-shell atoms, the atom EDM of Xe [1] and Hg [2] have been measured. Though the Hg experiment has set the record of being the most sensitive spectroscopy ever done, the result obtained is null and sets an upper bound to atomic Hg EDM as  $2.1 \times 10^{-28} ecm$ . Still, it has set bounds on the parameters in particle physics models [2]. Improving the accuracy further is an important challenge in atomic EDM experiments. Atomic Yb offer a possibility of achieving this by using the techniques of laser cooling and trapping. It is also desirable that the EDM measurements be done in other closed-shell atoms to verify the physical effects observed.

Atomic Yb also has the advantage of being relatively simple in level structure among the rare Earth elements. It has been studied theoretically using a variety of atomic many-body methods and there are ongoing experimental studies. The excitation energies has been studied using relativistic coupled-cluster method [3]; the hyperfine structure constants and electric-dipole transition properties have been studied using multireference relativistic many-body perturbation theory [4,5]; and the oscillator strength of some of the important transitions were investigated using multi-configuration relativistic Hartree-Fock [6]. The lifetime of some of the crucial levels have been measured experimentally [7] and atomic Yb has been laser cooled and trapped [8,9]. It is the candidate for the atomic EDM experiments using the methods of laser cooling and trapping of atoms which are in progress [10,11].

The P-T violating effects which can be probed using atomic Yb are the tensor pseudotensor (T-PT) electron-nucleus interaction [12] and the Schiff moment [13]. An observation of a finite EDM of atomic Yb could mean nonzero  $C_T$ , which is a signature of physics beyond the SM as  $C_T$  is zero within SM. Hence the theories which allow T-PT electron-nucleus interactions would play a role in understanding nature. The parameter  $C_T$  is extracted from the experimental result of atomic EDM by combining with the theoretical calculations. Accurate atomic theory calculations are needed to obtain precise  $C_T$ . The atomic EDM can also put bounds on the parameters of alternative models in particle physics.

The Schiff moment which arises due to either nucleon EDM or P-T violating interactions between the nucleons can also contribute to the Yb EDM and can be used to extract the nuclear P-T violation parameters. We have calculated the contribution to atomic Yb EDM from both these effects but in this paper we will present the result of our calculations for T-PT contribution alone, in a later paper we will present the result of our Schiff moment Computation.

The calculation of Yb EDM within a limited set of configuration state functions (CSFs) using diagonalization and Bloch equation based many-body perturbation theory ( MBPT) methods was reported in an earlier paper [14]. For convenient of reference this paper is called as paper-I hereafter. As a followup, in this paper we present results of calculations using much larger CSF space. In addition, we discuss the drawbacks common to the diagonalization and Bloch equation based perturbation methods, improvements are discussed and results of using these methods are presented. In this paper we present the method of the calculation.

## II. BLOCH EQUATION BASED MANY-BODY PERTURBATION THEORY

This section is a brief overview of the interaction used in the calculation and Bloch equation based MBPT. A detailed description of which are given in the paper-I. The effective T-PT electron-nucleus interaction Hamiltonian obtained by treating the nucleus nonrelativistically is

$$H_{\text{PTV}} = i2\sqrt{2}\left(C_T G_F\right)\left(\vec{I} \cdot \beta \vec{\alpha}\right) \rho_N(r), \quad (2.1)$$

where  $C_T$  is the T-PT electron-nucleus coupling constant,  $G_F$  is the Fermi coupling constant,  $\vec{I}$  is the nuclear spin,  $\beta$  and  $\alpha$  are the Dirac matrices and  $\rho_N(r)$  is the nuclear density. This interaction Hamiltonian is effective only within the nuclear region, where  $\rho_N(r)$  is non-zero. And the dependence on  $\vec{I}$  implies that it is observable only in odd isotopes of Yb which has nonzero  $\vec{I}$ . We use Fermi nuclear density model for our calculations.

The Bloch equation of an atom with unperturbed Hamiltonian  $H_0$  and the residual coulomb interaction  $V_{\text{es}}$  as the perturbation is

$$[\Omega_{\text{es}}, H_0] = V_{\text{es}}\Omega_{\text{es}} - \chi_{\text{es}} P V_{\text{es}} \Omega_{\text{es}}. \quad (2.2)$$

Where  $\Omega_{\text{es}}$  is the wave-operator,  $\chi_{\text{es}} = \Omega_{\text{es}} - 1$  is the correlation operator,  $P$  and  $Q$  are the projection operators of the model and complementary space. The first and second terms on the right hand side are the principal and renormalization terms respectively. Using Epstein-Nesbet(E-N) partitioning  $H_0$  and  $V_{\text{es}}$  can be defined in terms of a set of CSFs as

$$\begin{aligned} H_0 &= \sum_i \langle \Phi_i | H_{\text{atom}} | \Phi_i \rangle | \Phi_i \rangle \langle \Phi_i | + \sum_i \langle \bar{\Phi}_i | H_{\text{atom}} | \bar{\Phi}_i \rangle | \bar{\Phi}_i \rangle \langle \bar{\Phi}_i |, \\ V_{\text{es}} &= \sum_{ij} \langle \Phi_i | H_{\text{atom}} | \Phi_j \rangle | \Phi_i \rangle \langle \Phi_j | + \sum_{ij} \langle \bar{\Phi}_i | H_{\text{atom}} | \bar{\Phi}_j \rangle | \bar{\Phi}_i \rangle \langle \bar{\Phi}_j |, \end{aligned}$$

where  $H_{\text{atom}}$  is the Dirac-Coulomb atomic Hamiltonian, and  $\{|\Phi_i\rangle\}$  and  $\{|\bar{\Phi}_i\rangle\}$  are the even and odd parity CSF spaces respectively. The Dirac-Coulomb Hamiltonian of an atom with  $N$  electrons in atomic units (  $e = 1$ ,  $\hbar = 1$ , and  $m_e = 1$  ) is

$$H_{\text{atom}} = \sum_{i=1}^N \left( c\vec{\alpha}_i \cdot \vec{p}_i + (\beta_i - 1)c^2 - V_{\text{nuc}}(r_i) \right) + \frac{1}{2} \sum_{i,j}^{N,N} \frac{1}{r_{ij}}, \quad (2.3)$$

where  $\vec{\alpha}_i$  is the Dirac matrix,  $\vec{p}_i$  is the momentum of the electron and  $V_{\text{nuc}}$  is the nuclear potential. Introduce the P-T violating interaction Hamiltonian  $H_{\text{PTV}}$  as perturbation and define the total perturbation Hamiltonian  $V$  as

$$V = V_{\text{es}} + H_{\text{PTV}}, \quad (2.4)$$

The interaction Hamiltonian  $H_{\text{PTV}}$  can also be expressed in terms of CSFs as in  $H_0$  and  $V_{\text{es}}$ . Treating  $V$  as the perturbation and defining  $\Omega(\text{edm})$  as the total wave operator

$$\Omega(\text{edm}) = \Omega_{\text{es}} + \Omega_{\text{es,edm}}, \quad (2.5)$$

where  $\Omega_{\text{es}}$  remains the same and  $\Omega_{\text{es,edm}}$  is the wave-operator which has one order of  $H_{\text{PTV}}$  and all possible orders of  $V_{\text{es}}$  before and after  $H_{\text{PTV}}$ . The  $H_{\text{PTV}}$  is treated to first order since it scales as  $G_F$ , which is very small. The expression of the atomic EDM  $d_a$  is

$$d_a = \left\langle \Phi_0 \left| \Omega_{\text{es}}^\dagger \vec{D} \Omega_{\text{es,edm}} \right| \Phi_0 \right\rangle + \left\langle \Phi_0 \left| \Omega_{\text{es,edm}}^\dagger \vec{D} \Omega_{\text{es}} \right| \Phi_0 \right\rangle = \left\langle \Phi_0 \left| \vec{D}_{\text{eff}} \right| \Phi_0 \right\rangle, \quad (2.6)$$

where  $\vec{D}_{\text{eff}} = \Omega_{\text{es}}^\dagger \vec{D} \Omega_{\text{es,edm}} + \Omega_{\text{es,edm}}^\dagger \vec{D} \Omega_{\text{es}}$  is the effective atomic EDM operator. It is the dipole operator dressed with the all order residual coulomb interaction and one order of  $H_{\text{PTV}}$  arranged in all possible sequence. The Bloch equation based MBPT has been used for the calculation with a large CSFs space as it is more efficient in terms of execution time unlike the direct matrix diagonalization approaches.

### III. SIZE CONSISTENT THEORY IN CLOSED-SHELL SYSTEMS

An atomic many-body theory is size consistent if the properties calculated using it scales linearly as the number of the electrons. The diagonalization and the Bloch equation based methods are size consistent within a complete CSF space. But it is size inconsistent if the configuration space considered is incomplete. A consequence of incomplete cancellation of the unlinked terms, which scales nonlinearly to the number of electrons. The cancellation is complete when the CSF space is complete. To study atomic EDM which has important implications and small in magnitude it is preferable to use atomic-many body theory which is size-consistent even with an incomplete CSF space. It is also difficult to satisfy the condition of completeness for heavy atoms, which are important candidates for the atomic EDM experiments as the number of possible CSFs runs into millions for a moderate size orbital space.

#### A. Size Consistency with Linked Diagram Theorem

The wave-operator calculated using the Bloch equation within an incomplete CSF space is size-consistent if only the linked terms are retained [16]. The incomplete cancellation of the unlinked terms is then avoided

$$\left[ \Omega_{\text{es}}, H_0 \right] P = Q \left( V_{\text{es}} \Omega_{\text{es}} P - \chi_{\text{es}} P V_{\text{es}} \Omega_{\text{es}} P \right)_{\text{linked}} = Q \left( V_{\text{es}} \Omega_{\text{es}} P - \chi_{\text{es}} W \right)_{\text{linked}}, \quad (3.1)$$

where  $W = P V_{\text{es}} \Omega_{\text{es}} P$ . Redefine the wave-operator in terms of orders of excitation and consider only the single and double excitations. The wave-operator and correlation-operator are

$$\Omega_{\text{es}} = I + \Omega_{\text{es}}(1) + \Omega_{\text{es}}(2) = \sum_{m=0}^2 \Omega_{\text{es}}(m) \quad \text{and} \quad \chi_{\text{es}} = \sum_{m=1}^2 \Omega_{\text{es}}(m), \quad (3.2)$$

where  $m$  is the order of excitation. The closed-shell single and double excitation wave-operator diagrams are shown in Fig1. Similarly, the  $V_{\text{es}}$  diagrams are shown in Fig2. Unlike the single particle approach, the diagrams are used as representation of the physical effects and cannot be evaluated directly using the usual Goldstone rules as E-N partitioning is used. The  $W$  is the energy and hence a number for closed-shell systems. From the definitions

$$\left[ \Omega_{\text{es}}(m), H_0 \right] = Q \left( V_{\text{es}} + V_{\text{es}} \Omega_{\text{es}}(1) + V_{\text{es}} \Omega_{\text{es}}(2) - \Omega_{\text{es}}(m) W \right)_{m, \text{linked}}. \quad (3.3)$$

Let  $|\Phi_0\rangle$  be the reference configuration and  $\{|\Phi_\alpha\rangle\}$  be the configuration space spanned by singly and doubly excited configurations. The wave-operators can then be expressed as

$$\Omega_{\text{es}}(1) = \sum_{ar} \left| \Phi_a^r \right\rangle \left\langle \Phi_0 \right| x_a^r \quad \text{and} \quad \Omega_{\text{es}}(2) = \sum_{abrs} \left| \Phi_{ab}^{rs} \right\rangle \left\langle \Phi_0 \right| x_{ab}^{rs}. \quad (3.4)$$

Where  $x_a^r$  and  $x_{ab}^{rs}$  are the excitation amplitudes. For closed-shell systems with a single reference,  $W$  is just a number or closed diagrams. The term  $\Omega_{\text{es}} W$  is therefore unlinked and does not contribute to the linked Bloch equation. The one-body wave-operator equation is

$$\left[ \Omega_{\text{es}}(1), H_0 \right] P = \sum_{ar} \left[ \left\langle \Phi_a^r \right| V_{\text{es}} \left| \Phi_0 \right\rangle + \sum_{a'r'} \left\langle \Phi_a^r \right| V_{\text{es}} \left| \Phi_{a'}^{r'} \right\rangle x_{a'}^{r'} + \sum_{a'b'r's'} \left\langle \Phi_a^r \right| V_{\text{es}} \left| \Phi_{a'b'}^{r's'} \right\rangle x_{a'b'}^{r's'} \right]_{\text{linked}} \left| \Phi_a^r \right\rangle \left\langle \Phi_0 \right| \quad (3.5)$$

Similarly, the two-body wave-operator the equation is

$$\left[ \Omega_{\text{es}}(2), H_0 \right] P = \sum_{abrs} \left[ \langle \Phi_{ab}^{rs} | V_{\text{es}} | \Phi_0 \rangle + \sum_{a'r'} \langle \Phi_{ab}^{rs} | V_{\text{es}} | \Phi_{a'}^{r'} \rangle x_{a'}^{r'} + \sum_{a'b'r's'} \langle \Phi_{ab}^{rs} | V_{\text{es}} | \Phi_{a'b'}^{r's'} \rangle x_{a'b'}^{r's'} \right] \Big|_{\text{linked}} \Phi_{ab}^{rs} \rangle \langle \Phi_0 | \quad (3.6)$$

Introduce  $H_{\text{PTV}}$  as perturbation and redefine the perturbation Hamiltonian as  $V = V_{\text{es}} + H_{\text{PTV}}$ . The corresponding wave-operators are

$$\Omega(1) = \Omega_{\text{es}}(1) + \Omega_{\text{es,edm}}(1) \quad \text{and} \quad \Omega(2) = \Omega_{\text{es}}(2) + \Omega_{\text{es,edm}}(2). \quad (3.7)$$

Wave-operators  $\Omega_{\text{es}}(1)$  and  $\Omega_{\text{es}}(2)$  are same as before but  $\Omega_{\text{es,edm}}(1)$  and  $\Omega_{\text{es,edm}}(2)$  connect  $\{|\Phi_i\rangle\}$  to  $\{|\bar{\Phi}_i\rangle\}$ , where  $\{|\bar{\Phi}_i\rangle\}$  is the configuration space opposite in parity to  $|\Phi_0\rangle$ . Within the total configuration space  $\Omega_{\text{es,edm}}(1)$  and  $\Omega_{\text{es,edm}}(2)$  can be represented as

$$\Omega_{\text{es,edm}}(1) = \sum_{ar} |\bar{\Phi}_a^r\rangle \langle \Phi_0 | \bar{x}_a^r \quad \text{and} \quad \Omega_{\text{es,edm}}(2) = \sum_{abrs} |\bar{\Phi}_{ab}^{rs}\rangle \langle \Phi_0 | \bar{x}_{ab}^{rs} \quad (3.8)$$

The equations of  $\Omega_{\text{es,edm}}(1)$  is

$$\begin{aligned} \left[ \Omega_{\text{es,edm}}(1), H_0 \right] P = & \sum_{ar} \left[ \langle \bar{\Phi}_a^r | H_{\text{PTV}} | \Phi_0 \rangle + \sum_{a'r'} \langle \bar{\Phi}_a^r | H_{\text{PTV}} | \Phi_{a'}^{r'} \rangle x_{a'}^{r'} + \sum_{a'b'r's'} \langle \bar{\Phi}_a^r | H_{\text{PTV}} | \Phi_{a'b'}^{r's'} \rangle x_{a'b'}^{r's'} \right. \\ & \left. + \sum_{ct} \langle \bar{\Phi}_a^r | V_{\text{es}} | \bar{\Phi}_c^t \rangle \bar{x}_c^t + \sum_{cdtu} \langle \bar{\Phi}_a^r | V_{\text{es}} | \bar{\Phi}_{cd}^{tu} \rangle \bar{x}_{cd}^{tu} \right] \Big|_{\text{linked}} \bar{\Phi}_a^r \rangle \langle \Phi_0 | \end{aligned} \quad (3.9)$$

The wave-operator defined by equation (3.9) has only one order of  $H_{\text{PTV}}$  as terms of the form  $\langle \Phi_i | H_{\text{PTV}} | \bar{\Phi}_j \rangle \bar{x}$  are excluded. The equation of  $\Omega_{\text{PTV}}(2)$  is

$$\begin{aligned} \left[ \Omega_{\text{PTV}}(2), H_0 \right] P = & \sum_{abrs} \left[ \sum_{a'r'} \langle \bar{\Phi}_{ab}^{rs} | H_{\text{PTV}} | \Phi_{a'}^{r'} \rangle x_{a'}^{r'} + \sum_{a'b'r's'} \langle \bar{\Phi}_{ab}^{rs} | H_{\text{PTV}} | \Phi_{a'b'}^{r's'} \rangle x_{a'b'}^{r's'} + \sum_{ct} \langle \bar{\Phi}_{ab}^{rs} | V_{\text{es}} | \bar{\Phi}_c^t \rangle \bar{x}_c^t \right. \\ & \left. + \sum_{cdtu} \langle \bar{\Phi}_{ab}^{rs} | V_{\text{es}} | \bar{\Phi}_{cd}^{tu} \rangle \bar{x}_{cd}^{tu} \right] \Big|_{\text{linked}} \bar{\Phi}_{ab}^{rs} \rangle \langle \Phi_0 | \end{aligned} \quad (3.10)$$

The term  $\langle \bar{\Phi}_{ab}^{rs} | H_{\text{PTV}} | \Phi_0 \rangle$  does not contribute as the one-body interaction Hamiltonian  $H_{\text{PTV}}$  cannot create double excitations. The equations (3.5)–(3.10) are the required wave-operator equations.

## B. Size Consistency with Connected Diagrams

Consider the term  $\langle \Phi_{ab}^{rs} | V_{\text{es}} | \Phi_{a'}^{r'} \rangle x_{a'}^{r'}$  in (3.6) the diagrams of which are given in Fig.3. Among the diagrams (a) is linked but disconnected and remaining are connected. The disconnected diagrams in the wave-operator can introduce unlinked terms in the next iteration and hence a selection of only linked terms is required, this is difficult in terms of CSFs as all the contributions are combined. The other method of separating the wave-operator is in terms of connected cluster operators. It is easier to select connected terms, since it can be done without separating cluster operator into subcomponents. Consider the term  $\langle \Phi_{ab}^{rs} | V_{\text{es}} | \Phi_{a'}^{r'} \rangle x_{a'}^{r'}$  again, the disconnected contributions has  $a'$  and  $r'$  in  $|\Phi_{ab}^{rs}\rangle$  and excitation is through the one-body part in  $V_{\text{es}}$ , avoiding these terms make the contributions from  $\langle \Phi_{ab}^{rs} | V_{\text{es}} | \Phi_{a'}^{r'} \rangle x_{a'}^{r'}$  connected. The third term in (3.10) still has disconnected terms but using the the same method these can be removed. After these modifications all the terms of the cluster equations are connected. To distinguish from the linked diagram excitation operators define the cluster-operator as  $T_n$ , then

$$T_n = \left( \Omega(n) \right)_{\text{conn}} \quad \text{and} \quad T = \sum_{n=1}^N T_n \quad (3.11)$$

Taking only the linear terms of one and two-particle cluster-operators, the wave-operator is

$$\Omega_{\text{es}} = 1 + T_{\text{es}}(1) + T_{\text{es}}(2) \quad \text{and} \quad W = V_{\text{es}} T. \quad (3.12)$$

The wave-operator  $\Omega_{\text{es}}$  is approximated by the linear cluster terms for the following reasons:

1. The correlation introduced by  $T_1^2$  is very small compared to the contribution from  $T_2$ , which represents a large part of the electron-electron correlation effect.
2. Among the four-body cluster operators  $T_2^2$  is the major contributor but in the present formalism this term can not be included as the CSF coupling is not in particle-hole form.
3. Though  $T_1$  does not contribute significantly to the electron-electron correlation it is important since  $H_{\text{PTV}}$  and the dipole operators are single-electron operators.

The equation of the cluster-operator treating  $V_{\text{es}}$  as the perturbation is

$$\left[T_{\text{es}}, H_0\right]P = \left(QV_{\text{es}}\Omega_{\text{es}}P - \chi_{\text{es}}WP\right)_{\text{conn}} \quad (3.13)$$

In closed-shell systems  $\chi_{\text{es}}W$  is always disconnected and do not contribute to the cluster equation

$$\left[T_{\text{es}}, H_0\right]P = \left(QV_{\text{es}}\Omega_{\text{es}}P\right)_{\text{conn}}. \quad (3.14)$$

These are the CEPA-0 equations and do not include the EPV diagrams. The linked EPV diagrams should be avoided but unlinked EPV terms should be retained. After suitable transformations the unlinked EPV terms can be converted into connected terms [18], thus the cluster-operator equation is

$$\left[T_{\text{es}}, H_0\right]P = \left(QV_{\text{es}}\Omega_{\text{es}}P\right)_{\text{linked}}^{\text{EPV}} + \left(QV_{\text{es}}\Omega_{\text{es}}P\right)_{\text{conn}}^{\text{EPO}}. \quad (3.15)$$

Where the first term is EPV and second term is non-EPV. By rearranging

$$\left(QV_{\text{es}}\Omega_{\text{es}}P\right)_{\text{linked}}^{\text{EPV}} = -\left(Q\chi_{\text{es}}WP\right)^{\text{EPV}}. \quad (3.16)$$

Then, the cluster-operator equations are

$$\left[T_{\text{es}}, H_0\right]P = \left(QV_{\text{es}}\Omega_{\text{es}}P\right)_{\text{conn}}^{\text{EPO}} - \left(Q\chi_{\text{es}}WP\right)^{\text{EPV}} \quad (3.17)$$

The one-particle cluster operator equation is

$$\left[T_{\text{es}}(1), H_0\right]P = \sum_{ar} \left[ \left\langle \Phi_a^r | V_{\text{es}} | \Phi_0 \right\rangle + \sum_{a'r'} \left\langle \Phi_a^r | V_{\text{es}} | \Phi_{a'}^{r'} \right\rangle \mathcal{T}_{a'}^{r'} + \sum_{a'b'r's'} \left\langle \Phi_a^r | V_{\text{es}} | \Phi_{a'b'}^{r's'} \right\rangle \mathcal{T}_{a'b'}^{r's'} - \left( \mathcal{T}_a^r W \right)^{\text{EPV}} \right] \left| \Phi_a^r \right\rangle \left\langle \Phi_0 \right|. \quad (3.18)$$

The cluster amplitudes are denoted by  $\mathcal{T}$  to distinguish from the one-particle cluster amplitudes represented by  $t$ . Here the calculation is using CSFs and  $\mathcal{T}_a^r$  is the amplitude of the cluster operator which excites the reference CSF  $|\Phi_0\rangle$  to the CSF  $|\Phi_a^r\rangle$ . Similarly, the two-particle cluster amplitudes can be defined.

$$\left[T_{\text{es}}(2), H_0\right]P = \sum_{abrs} \left[ \left\langle \Phi_{ab}^{rs} | V_{\text{es}} | \Phi_0 \right\rangle + \sum_{a'r'} \left\langle \Phi_{ab}^{rs} | V_{\text{es}} | \Phi_{a'}^{r'} \right\rangle \mathcal{T}_{a'}^{r'} + \sum_{a'b'r's'} \left\langle \Phi_{ab}^{rs} | V_{\text{es}} | \Phi_{a'b'}^{r's'} \right\rangle \mathcal{T}_{a'b'}^{r's'} - \left( \mathcal{T}_{ab}^{rs} W \right)^{\text{EPV}} \right] \left| \Phi_{ab}^{rs} \right\rangle \left\langle \Phi_0 \right|. \quad (3.19)$$

Similarly, the PT-violating cluster-operators  $T_{\text{PTV}}$  are evaluated using the equations

$$\begin{aligned} \left[T_{\text{es,edm}}(1), H_0\right]P = & \sum_{ar} \left[ \left\langle \overline{\Phi}_a^r | H_{\text{PTV}} | \Phi_0 \right\rangle + \sum_{a'r'} \left\langle \overline{\Phi}_a^r | H_{\text{PTV}} | \Phi_{a'}^{r'} \right\rangle \mathcal{T}_{a'}^{r'} + \sum_{a'b'r's'} \left\langle \overline{\Phi}_a^r | H_{\text{PTV}} | \Phi_{a'b'}^{r's'} \right\rangle \mathcal{T}_{a'b'}^{r's'} \right. \\ & \left. + \sum_{ct} \left\langle \overline{\Phi}_a^r | V_{\text{es}} | \overline{\Phi}_c^t \right\rangle \overline{\mathcal{T}}_c^t + \sum_{cdtu} \left\langle \overline{\Phi}_a^r | V_{\text{es}} | \overline{\Phi}_{cd}^{tu} \right\rangle \overline{\mathcal{T}}_{cd}^{tu} - \left( \overline{\mathcal{T}}_a^r W \right)^{\text{EPV}} \right] \left| \overline{\Phi}_a^r \right\rangle \left\langle \Phi_0 \right| \end{aligned} \quad (3.20)$$

and

$$\begin{aligned} \left[ T_{\text{es,edm}}(2), H_0 \right] P = & \sum_{abrs} \left[ \sum_{a'b'r's'} \langle \bar{\Phi}_{ab}^{rs} | H_{\text{PTV}} | \Phi_{a'b'}^{r's'} \rangle \mathcal{T}_{a'b'}^{r's'} + \sum_{ct} \langle \bar{\Phi}_{ab}^{rs} | V_{\text{es}} | \bar{\Phi}_c^t \rangle \bar{t}_c^t \right. \\ & \left. + \sum_{cdtu} \langle \bar{\Phi}_{ab}^{rs} | V_{\text{es}} | \bar{\Phi}_{cd}^{tu} \rangle \bar{\mathcal{T}}_{cd}^{tu} - \left( \bar{\mathcal{T}}_{ab}^{rs} W \right)^{\text{EPV}} \right] | \bar{\Phi}_{ab}^{rs} \rangle \langle \Phi_0 | \end{aligned} \quad (3.21)$$

Using the cluster-operators

$$\Omega_{\text{es,edm}} = \Omega_{\text{es,edm}}(1) + \Omega_{\text{es,edm}}(2). \quad (3.22)$$

The atomic EDM  $d_a$  can be calculated using the operators as

$$d_a = \langle \Phi_0 | \bar{D}_{\text{eff}} | \Phi_0 \rangle, \quad (3.23)$$

where  $\bar{D}_{\text{eff}} = \Omega_{\text{es}}^\dagger \bar{D} \Omega_{\text{es,edm}} + \Omega_{\text{es,edm}}^\dagger \bar{D} \Omega_{\text{es}}$  is same as before except that the wave-operator is now in terms of connected clusters. The cluster equations are similar to the CEPA-2 equations [19,21], the explicit CEPA-0 equations are same as these equations without the EPV terms.

#### IV. ANALYSIS OF THE CLUSTER EQUATIONS

The cluster based formalism is not an order by order formalism but an iterative scheme where the Bloch equation is defined in orders of excitations rather than the orders of perturbation. It is possible to separate the contributions from various many-body effects cleanly using Moller-Plesset partitioning and an added advantage is the one-to-one correspondence with the diagrams using Goldstone evaluation rules. Such an approach has been used [20] to calculate parity non-conservation in atomic cesium to very high accuracy. The E-N partitioning mixes the contributions, but it has the advantage of capturing the static correlation effects very effectively. The CEPA-0 equations are exactly the linearized singles and doubles coupled cluster equations, the CEPA-2 equations includes a class of non-linear terms.

##### A. The Singly Excited Amplitude Cluster Equation

The diagrammatic representation of the principal terms in (3.18) are shown in Fig.4. The contribution from each of the diagrams are as described:

1. Diagram (a) contributes to the first term  $\langle \Phi_a^r | H_{\text{es}} | \Phi_0 \rangle$  of the cluster equation and is independent of any cluster amplitudes. It is an important term as the iteration proceeds from this term.
2. The diagrams (b),(c),(d),(e) and (f) contribute to the second term  $\langle \Phi_a^r | H_{\text{es}} | \Phi_{a'}^{r'} \rangle \mathcal{T}_{a'}^{r'}$  and the  $V_{\text{es}}$  matrix element is coupled with the single excitation cluster amplitude. These start contributing from the second iteration, where the cluster amplitude  $\mathcal{T}_{a'}^{r'}$  is just the matrix element  $\langle \Phi_{a'}^{r'} | V_{\text{es}} | \Phi_0 \rangle$  in the first iteration.
3. Diagrams (g),(h),(i) and (j) contribute to the third term  $\langle \Phi_a^r | V_{\text{es}} | \Phi_{a'b'}^{r's'} \rangle \mathcal{T}_{a'b'}^{r's'}$  and couple the double excitation cluster amplitude with the  $V_{\text{es}}$  matrix element. Similar to the second term, these diagrams start contributing from the second iteration.

Consider the diagrams (c) and (e), though they resemble the Hartree-Fock potential scattering diagram these are very different. Consider the the bubble part of the diagram (c), it is summed over the occupied orbitals common to both the initial and the final CSFs in the matrix element of  $V_{\text{es}}$ . An example in Yb is if the initial and final CSFs are  $|\Phi_{a'b'}^{r's'}\rangle = |7s^2\rangle$  and  $|\Phi_{ab}^{rs}\rangle = |7s8s\rangle$  respectively, the bubble part in (c) has all the occupied orbitals except the 6s orbital. This is because both the CSFs do not have 6s, where as in the Hartree-Fock scattering diagram the bubble should have contribution from all the occupied orbitals. A similar description is true of diagrams (d) and (f) too.

The term  $(\mathcal{T}_a^r W)^{\text{EPV}}$  picks up the effect of the non-linear terms  $T_{\text{es}}(1)^2$  and  $T_{\text{es}}(1)T_{\text{es}}(2)$ , which have  $T_{\text{es}}(1)$  amplitudes. This implies that the wave-operator assumes the form

$$\Omega_{\text{es}} = 1 + T_{\text{es}}(1) + T_{\text{es}}(2) + \left[ T_{\text{es}}(1)T_{\text{es}}(1) + T_{\text{es}}(1)T_{\text{es}}(2) + T_{\text{es}}(2)T_{\text{es}}(2) \right]^{\text{EPV}} \quad (4.1)$$

Terms which are not included in the single excitation cluster amplitude equation are

$$\left[ T_{\text{es}}(1)T_{\text{es}}(1) + T_{\text{es}}(1)T_{\text{es}}(2) + T_{\text{es}}(2)T_{\text{es}}(2) \right]^{\text{EPO}}. \quad (4.2)$$

A later section describes the method to choose EPV terms from the renormalization part.

## B. The Doubly Excited Cluster Amplitude Equation

The diagrams of the principal terms of the double excitation cluster amplitude (3.19) are shown in Fig.5. The first term is similar to that of the single excitation cluster amplitude equation. The second term can be separated as

$$\begin{aligned} \sum_{a'r'} \langle \Phi_{ab}^{rs} | V_{\text{es}} | \Phi_{a'}^{r'} \rangle \mathcal{T}_{a'}^{r'} &= \langle \Phi_{ab}^{rs} | V_{\text{es}} | \Phi_a^r \rangle \mathcal{T}_a^r + \sum_{a' \neq a, b} \langle \Phi_{ab}^{rs} | V_{\text{es}} | \Phi_{a'}^r \rangle \mathcal{T}_{a'}^r + \sum_{r' \neq r, s} \langle \Phi_{ab}^{rs} | V_{\text{es}} | \Phi_a^{r'} \rangle \mathcal{T}_a^{r'} \\ &+ \sum_{a' \neq a, b} \langle \Phi_{ab}^{rs} | V_{\text{es}} | \Phi_{a'}^s \rangle \mathcal{T}_{a'}^s + \sum_{r' \neq r, s} \langle \Phi_{ab}^{rs} | V_{\text{es}} | \Phi_b^{r'} \rangle \mathcal{T}_b^{r'} \end{aligned}$$

The first term on the right hand side has connected as well as disconnected terms, from which only the connected terms should be retained. The remaining terms are connected and hence linked too since the conditions  $a' \neq a, b; r' \neq r, s$  exclude the disconnected terms. Then

$$\sum_{a'r'} \langle \Phi_{ab}^{rs} | V_{\text{es}} | \Phi_{a'}^{r'} \rangle \mathcal{T}_{a'}^{r'} = \langle \Phi_{ab}^{rs} | V_{\text{es}} | \Phi_a^r \rangle \mathcal{T}_a^r + \sum_{r' \neq r, s} \left( \delta_{a'a} + \delta_{a'b} \right) \langle \Phi_{ab}^{rs} | V_{\text{es}} | \Phi_{a'}^{r'} \rangle \mathcal{T}_{a'}^{r'} + \sum_{a' \neq a, b} \left( \delta_{r'r} + \delta_{r's} \right) \langle \Phi_{ab}^{rs} | V_{\text{es}} | \Phi_{a'}^{r'} \rangle \mathcal{T}_{a'}^{r'} \quad (4.3)$$

Similarly, the third term can be expanded to

$$\begin{aligned} \sum_{a'b'r's'} \langle \Phi_{ab}^{rs} | V_{\text{es}} | \Phi_{a'b'}^{r's'} \rangle \mathcal{T}_{a'b'}^{r's'} &= \sum_{b' \neq a, b} \sum_{r' \neq r, s} \left[ \langle \Phi_{ab}^{rs} | V_{\text{es}} | \Phi_{ab'}^{rs'} \rangle \mathcal{T}_{ab'}^{rs'} + \sum_{s' \neq r, s} \left[ \langle \Phi_{ab}^{rs} | V_{\text{es}} | \Phi_{ab}^{r's'} \rangle \mathcal{T}_{ab}^{r's'} + \sum_{s' \neq r, s} \langle \Phi_{ab}^{rs} | V_{\text{es}} | \Phi_{ab}^{r's'} \rangle \mathcal{T}_{ab}^{r's'} \right] \right] \\ &+ \sum_{a' \neq a, b} \left[ \langle \Phi_{ab}^{rs} | V_{\text{es}} | \Phi_{a'b}^{rs} \rangle \mathcal{T}_{a'b}^{rs} + \sum_{b' \neq a, b} \langle \Phi_{ab}^{rs} | V_{\text{es}} | \Phi_{a'b'}^{rs} \rangle \mathcal{T}_{a'b'}^{rs} \right], \end{aligned}$$

where all the terms are connected. The triply and quadruply excited terms are excluded. Each of the diagrams has an exchange diagram too. Terms corresponding to each of the diagrams are:

1. Diagram (a) correspond to the first term in the cluster equation and has no dependence on any of the cluster amplitude.
2.  $\langle \Phi_{ab}^{rs} | V_{\text{es}} | \Phi_a^r \rangle \mathcal{T}_a^r$  contribute to diagrams (b) and (c). The final CSF in this term has a hole-particle pair in common with the cluster amplitude.
3.  $(\delta_{a'a} + \delta_{a'b}) \langle \Phi_{ab}^{rs} | V_{\text{es}} | \Phi_{a'}^{r'} \rangle \mathcal{T}_{a'}^{r'}$  contribute to diagram (c). Though the topology of the diagram is same as that of  $\langle \Phi_{ab}^{rs} | V_{\text{es}} | \Phi_a^r \rangle \mathcal{T}_a^r$ , it is an EPO diagram. The  $V_{\text{es}}$  interaction changes the state of the particle and picks up a part of core-virtual correlation effect, which can be identified as core-polarization.
4.  $(\delta_{r'r} + \delta_{r's}) \langle \Phi_{ab}^{rs} | V_{\text{es}} | \Phi_{a'}^{r'} \rangle \mathcal{T}_{a'}^{r'}$  contribute to diagram (b). This also has similar topology with  $\langle \Phi_{ab}^{rs} | V_{\text{es}} | \Phi_a^r \rangle \mathcal{T}_a^r$  but is again an EPO diagram, where there is a change of the hole state and correspond to core-core correlation effect.
5.  $\langle \Phi_{ab}^{rs} | V_{\text{es}} | \Phi_{ab'}^{rs'} \rangle \mathcal{T}_{ab'}^{rs'}$  contribute to diagram (h) and (i). These are EPO diagrams where a hole-particle change to another hole-particle pair. These contribute to the core-virtual correlation effects.
6. The term  $\langle \Phi_{ab}^{rs} | V_{\text{es}} | \Phi_{ab}^{r's'} \rangle \mathcal{T}_{ab}^{r's'}$  contribute to diagrams (f) and (g). These are EPO diagrams where one of the particle states in  $\mathcal{T}_{ab}^{r's'}$  is excited to another particle state. This can also contribute to EPV diagrams of the first kind, if it is a hole-line EPV diagram then it will correspond to (h) and (i) and if it is particle line EPV then diagram (j).

7.  $\langle \Phi_{ab}^{rs} | V_{es} | \Phi_{ab}^{r's'} \rangle \mathcal{T}_{ab}^{r's'}$  contribute to diagram (j). This is a double excitation where the particle states from the cluster amplitude  $\mathcal{T}_{ab}^{r's'}$  are excited to different particle states but the hole states remain intact. These terms capture the virtual-virtual correlation effects.
8.  $\langle \Phi_{ab}^{rs} | V_{es} | \Phi_{a'b}^{rs} \rangle \mathcal{T}_{a'b}^{rs}$  contribute to diagram (d) and (e). These diagrams correspond to a change of the hole state and are EPO diagrams which capture the single-body hole-hole interaction component. This term can also contribute EPV diagrams, the hole line EPV diagram arising from this term is (k) and the particle line EPV diagrams are (h) and (i).
9.  $\langle \Phi_{ab}^{rs} | V_{es} | \Phi_{a'b'}^{rs} \rangle \mathcal{T}_{a'b'}^{rs}$  contribute to (j) and is a hole-hole correlation term.

Thus terms in the cluster equation contribute to different physical effects. So far only the first three terms in the cluster equation have been considered. The last term in the doubly excited cluster amplitude  $(\mathcal{T}_{ab}^{rs} W)^{\text{EPV}}$  is a renormalization term. It picks up a set of terms non-linear in cluster amplitude

$$T_{es}(1)T_{es}(2) + T_{es}(2)T_{es}(2). \quad (4.4)$$

These pick up a class of EPV terms which are non-linear in cluster amplitudes. Consider the expression of  $W$

$$W = PV_{es} \left( T_{es}(1) + T_{es}(2) \right) P. \quad (4.5)$$

The term  $T_{es}(1)T_{es}(2)$  is picked up through  $PV_{es}T_{es}(1)P$  in  $W$ , which implies that  $(\mathcal{T}_{ab}^{rs} PV_{es} T_{es}(1))^{\text{EPV}}$  can have one hole(particle) EPV line or a pair of hole-particle EPV lines. Whereas in the single excitation cluster amplitude equation, the contribution from  $T_{es}(1)T_{es}(2)$  is captured through the term  $(\mathcal{T}_a^r PV_{es} T_{es}(2))^{\text{EPV}}$  in  $(\mathcal{T}_a^r W)^{\text{EPV}}$ . But the number of EPV hole-lines or EPV particle-lines are the same in both. In general the number of EPV hole-lines and particle-lines in  $(T_{es}(n)PV_{es}T_{es}(m)P)^{\text{EPV}}$  is limited by the  $V_{es}$  if  $m, n > 2$  and by the cluster amplitudes if  $m < 2$  or  $n < 2$ . Although  $T_{es}(1)T_{es}(2)$  is included in the single as well as the double excitation cluster amplitudes the topology of the diagrammatic representations are different. Diagrams from  $(\mathcal{T}_a^r W)^{\text{EPV}}$  has only a pair of hole-particle lines where as  $(\mathcal{T}_{ab}^{rs} W)^{\text{EPV}}$  has two pairs of hole-particle lines.

### C. Selection of EPV Terms and Connected Terms

The terms linear in cluster amplitude cannot violate Pauli exclusion principal. It is possible only when there are CSFs which are EPV, which is not possible. The EPV diagrams arise from renormalization terms, which are non-linear in cluster amplitude. The diagrams representing the renormalization terms are the cluster diagrams multiplied by the energy diagrams and hence unlinked but these can suitably be rearranged to yield connected diagrams.

To select the EPV terms all the orbitals are tagged with labels which are prime numbers. The CSFs are also assigned a number which is the product of the prime numbers corresponding to the labels of the holes and particles of the CSFs. Consider a doubly excited CSF  $|\Phi_{ab}^{rs}\rangle$ , the prime numbers  $n_a, n_b, n_r$  and  $n_s$  be the labels of the hole and particle states and  $\mathcal{N}_{ab}^{rs}$  their product, these five numbers identify the CSF. However, only three if the CSF is singly excited. To maintain consistency the remaining two indices are filled with another prime number not used in labeling the orbitals, let this number be  $N_P$  but set the corresponding multiplying factor in  $n$  as unity. According to this scheme, the ground/reference state of Yb is identified by  $N_P, N_p, N_p, N_p$  and 1. Similarly, labels are also given to the cluster amplitudes.

The terms to retain from  $(\mathcal{T}_a^r W)^{\text{EPV}}$  are those having CSFs in  $W$  identified by  $\mathcal{N}$  which can be divided by one or more of the numbers identifying hole(particle) of the cluster amplitude  $\mathcal{T}$ . The number of possible division is the number of common hole/particle lines between  $\mathcal{T}$  and  $W$ . During the selection process division by  $N_p$  should be discarded as this does not represent any hole of particle states and this is automatically achieved as the corresponding multiplying factor in  $n$  is unity. The advantage of this scheme is that it reduces the number of operations required in the selection process.

The term  $\langle \Phi_{ab}^{rs} | V_{es} | \Phi_{a'}^{r'} \rangle \mathcal{T}_{a'}^{r'}$  of the doubly excited cluster amplitude equation has disconnected components if both the hole and particle states in the initial CSF are present in the final CSF. These are discarded and only the connected components are chosen. This can be implemented while calculating the matrix elements of  $V_{es}$ . During the matrix element calculation the total number of hole states of the initial and final CSFs is calculated. If this is equal to three then these contribute to  $\langle \Phi_{ab}^{rs} | V_{es} | \Phi_{a'}^{r'} \rangle \mathcal{T}_{a'}^{r'}$ . In the next step the connected component is chosen by selecting the  $V_{es}$  matrix element which has  $r'$ . Then the doubly excited cluster amplitude equation has only connected components. However the discarded components are disconnected but linked.



## V. THE CONFIGURATION SPACE CONSIDERED

The configuration space is spanned by the CSFs constructed from the  $V^{N-1}$  orbitals. The CSFs are generated by single or double excitations from the occupied orbitals to the bound and the continuum virtual orbitals in all possible ways such that it yields the required final angular momentum. For the single reference MBPT, the reference CSF of Yb is  $|6s^2\rangle$ , which be referred as  $|\Phi_0\rangle$ . Hence the occupied orbitals are  $(1-6)s, (2-5)p^*, (2-5)p, (3-4)d^*, (3-4)d, 4f^*$  and  $4f$  respectively. The CSF space generated is not a complete active space but complete for the single and double excitations from the most important outer occupied orbitals within the orbital orbital space. The occupied-orbital shells of the configurations that has been considered are

$$\begin{aligned} \text{single excitation: } & |4f^*6\ 4f^86s\rangle, |4f^*5\ 6s^2\rangle |4f^76s^2\rangle, |5p^*1\ 6s^2\rangle |5p^36s^2\rangle \text{ and } |5s^16s^2\rangle \\ \text{double excitation: } & |4f^*6\ 4f^8\rangle, |4f^*5\ 6s\rangle |4f^76s\rangle, |4f^*4\ 6s^2\rangle, |4f^66s^2\rangle, |4f^*5\ 4f^76s^2\rangle |5p^*1\ 6s\rangle, |5p^36s\rangle, \\ & |5p^*1\ 4f^56s^2\rangle, |5p^34f^5\ 6s^2\rangle, |5p^*3\ 4f^56s^2\rangle, |5p^34f^56s^2\rangle, |5s^16s\rangle, |5s^14f^*5\ 6s^2\rangle, |5s^14f^76s^2\rangle, \\ & |5s^15p^*1\ 6s^2\rangle \text{ and } |5s^15p^36s^2\rangle. \end{aligned}$$

The remaining electrons are distributed among the virtual orbitals in all possible ways. From all the CSFs only the  $J=0$  even parity and  $J=1$  odd parity CSFs are chosen. The number of non-relativistic CSFs generated are given in Table I. Although not included in the table, CSFs with excitations from  $5s$  are also included in the CSF space.

The total number of odd and even parity CSFs with bound virtual orbitals are 9930 and 17087 respectively. The modulus of the EN-partitioned energies of the CSFs—the diagonal Hamiltonian matrix elements—are as shown in the histograms Fig. 4. The two histograms are plotted such the the lowest  $|E|$  is shifted to zero and the the range between the lowest and the highest are divided into ten units. The zero on  $|E|$  axis are 14064.9531 and 14065.0068 hartrees for the even and odd parity CSFs respectively. Similarly, the highest  $|E|$  are 14067.6720 and 14067.5996 hartrees respectively. From the histogram, the number of CSFs with low and high energies are less whereas the number of the configurations that can give the intermediate energy are large. As a result the perturbation series converges fast as only a few of the configurations are quite close to  $|\Phi_0\rangle$  and the energy separation with the rest of the CSFs is quite large.

Number of odd parity CSFs in the intermediate energy is more than the even parity as the odd parity configuration space can have many possible intermediate couplings to give  $J=1$ , to limit the number of CSFs within the memory limitations a selection of CSFs is done. The double excitations to  $d$  and  $f$  symmetries above the energy of the converged orbitals are not included. Another constraint on the choice of configurations is: there shouldn't be more than four open shells in the non-relativistic notation and eight in the relativistic form, choosing only singly and doubly excited configurations satisfies this condition for a closed-shell atom like Yb. This constraint is due to the angular co-efficient computation program.

## VI. RESULTS

The atomic Yb EDM is calculated using the Bloch equation based MBPT and the size-consistent CEPA equations. As a part of the calculation the ground state energy is also computed. The results with different methods are given in the following sections.

### A. Bloch Equation Based MBPT

#### 1. Calculation of $\Omega_{\text{es}}$ and $E_0$

Using the wave-operator  $\Omega_{\text{es}}$  the ground state wave-function  $|\Psi_0\rangle$  and energy  $E_0$  are

$$|\Psi_0\rangle = \frac{\Omega_{\text{es}}|\Phi_0\rangle}{\langle\Phi_0|\Omega_{\text{es}}^\dagger\Omega_{\text{es}}|\Phi_0\rangle} \quad \text{and} \quad E_0 = \langle\Phi_0|V_{\text{es}}\Omega_{\text{es}}|\Phi_0\rangle. \quad (6.1)$$

The denominator in the expression of  $|\Psi_0\rangle$  is the normalization factor. The first order energy correction of the ground state is zero Since the calculations are using the EN-partitioned Hamiltonian.

The even parity CSF space of the calculation is spanned by 9930 CSFs, of which core part of first 4435, 4436-9094 and remaining CSFs are  $|4f^{14}6s\rangle$ ,  $|4f^{14}\rangle$ ,  $|4f^{13}6s^2\rangle|4f^{13}6s\rangle$  and  $|4f^{12}6s^2\rangle$ , and  $|5p^54f^{14}6s^2\rangle$ ,  $|5p^54f^{14}6s\rangle$  and  $|5p^54f^{13}\rangle$ , and  $|5s5p^64f^{14}6s^2\rangle$  respectively. Using this set of CSFs the ground state wave-function is

$$\begin{aligned} |\Psi_0\rangle = & 0.9251\ 23|6s^2\rangle + 0.1172\ 17|6p^*{}^2\rangle + 0.1169\ 21|6s7s\rangle + 0.0996\ 76|6p^2\rangle \\ & -0.0600\ 60|5d^2\rangle + 0.0568\ 61|6p7p\rangle - 0.0497\ 43|5d^*{}^2\rangle + 0.0480\ 54|6p^*7p^*\rangle \\ & +0.0443\ 18|6p8p\rangle - 0.0442\ 15|6s8s\rangle - 0.0320\ 73|5d6d\rangle + \dots \end{aligned}$$

Where only the ten important CSFs are given explicitly and the normalization constant is 1.0809 37. As expected, the most important CSFs in  $|\Psi_0\rangle$  are doubly excited except for  $|6s7s\rangle$ , which is a singly excited CSF and does not interact very strongly with the ground state CSF  $|6s^2\rangle$  but contributes significantly by correlation through other CSFs when the residual interaction is taken to higher orders. Values of  $E_0$  with increasing size of the even CSF space is given in TableII. CSFs are added to the calculation in sequence of excitations from the deeper core orbitals. As the size of the CSF space is increased more complicated many-body effects are included in the computation.

An important quantity that can be extracted from TableII is the change in  $E_0$ . Define the correlation energy  $\Delta E_0$  as the energy difference between the CSF energy of  $|6s^2\rangle$  and the energy calculated using the CSFs in the even-parity CSF space. From the plot of  $\Delta E_0$  in Fig7a it is evident that the change in the ground state ASF energy is not uniform but in steps interrupted by regions of very minimal changes. Most significant changes of  $\Delta E_0$  occur while increasing the CSFs from 100 to 500, from 1000 to 2000 and from 6435 to 7435 CSFs respectively. These changes are not the combined effect of all the CSFs added but due to a few important ones. The largest change of  $\Delta E_0$  is while increasing from 1000 to 2000 CSFs which corresponds to contribution from the core configuration  $|4f^{14}\rangle$ , that is double excitation from the  $6s$  orbital shell. The remaining two are due to the core configurations  $|4f^{13}6s\rangle$  and  $|5p^56s\rangle$ . Each contribute  $-0.0041\ 82$ ,  $-0.0179\ 26$  and  $-0.0045\ 07$  hartrees respectively, the combined effect adds to 81.20% of the total correlation energy  $-0.0304\ 50$  hartrees. From these it can be concluded that, the most important CSFs contributing to the correlation energy have core configurations  $|4f^{13}6s\rangle$ ,  $|4f^{14}\rangle$  and  $|5p^56s\rangle$ . As to be expected the doubly excited CSFs are most important to capture the correlation effects and the low lying double excitations from  $6s$  orbital shell has the most significant contribution to correlation energy, it contributes 54.74% of the correlation energy.

The plot (b) in Fig:7 indicates the need to include  $V_{es}$  to high orders to capture the correlation effects accurately. From the graph the correlation effect due to two order of  $V_{es}$  is  $-0.0436\ 033$  hartrees and decreases in magnitude monotonically till fourth order to  $-0.0306\ 67$ hartrees but increases in the fourth order to  $-0.0343\ 38$ hartrees. This trend of oscillation about the final value of  $\Delta E_0$  continues till convergence. The cycle of the oscillation has a period of four orders, that is in four orders it goes to the same side of the final value of  $\Delta E_0$  and the amplitude of the oscillation decreases with each cycle. Over all, the value of  $\Delta E_0$  behaves like a damped oscillator with a cycle of four orders. If  $E_0$  is calculated by truncating the perturbation to the first few orders where the amplitude of oscillation is quite significant the value of  $\Delta E_0$  can be erroneous.

The Fig.8 shows the trend of wave-operator convergence. The first graph Fig.8a is the value of the convergence criteria plotted against the order of perturbation and second graph Fig.8b is  $\log_{10}$  of the convergence criteria plotted against the order of perturbation. From the first graph it is evident that the convergence criteria begins with a small value but as shown in the second graph in terms of order of magnitude, the convergence is not so fast. The convergence is monotonic with very regular fluctuations. The wave-operator  $\Omega_{es}$  is stored in an order by order sequence. These are accessed as and when required during the calculation of  $\Omega_{es,edm}$ .

## 2. Calculation of $\Omega_{es,edm}$ and $d_a$

The wave-operator  $\Omega_{es,edm}$  is calculated introducing the interaction Hamiltonian  $H_{pTV}$  and adding opposite parity CSFs to the CSF space. Once  $H_{pTV}$  is applied to the wave-operator  $\Omega_{es}$ , it maps onto the odd-parity component of the CSF space and can never be mapped back to the even-parity space as  $H_{pTV}$  is treated to first order only. This is followed by a sequence of residual coulomb interaction  $V_{es}$ , which accounts for the correlation effects within the odd-parity sub-space. In sum total it is a sequence of perturbations applied to the ground state CSF  $|6s^2\rangle$ , where  $H_{pTV}$  is sandwiched between all possible arrangements of  $V_{es}$ . After the wave-operator  $\Omega_{es,edm}$  is calculated, the mixed parity ground state wave-function  $|\tilde{\Psi}_0\rangle$  can be written in terms of the wave-operators  $\Omega_{es}$  and  $\Omega_{es,edm}$  as

$$|\tilde{\Psi}_0\rangle = |\Psi_0\rangle + |\Psi_{corr}^0\rangle = \left( \Omega_{es} + \Omega_{es,edm} \right) |\Phi_0\rangle \quad (6.2)$$

The value of  $d_a$  can be calculated using the expression

$$d_a = \langle \tilde{\Psi}_0 | \vec{D} | \tilde{\Psi}_0 \rangle = 2 \langle \Phi_0 | \Omega_{\text{es}}^\dagger \vec{D} \Omega_{\text{es,edm}} | \Phi_0 \rangle \quad (6.3)$$

Choosing the odd parity CSF as mentioned in Sec. V the correction to the ground state  $|\Psi_0\rangle$  from the opposite parity sub-space due to  $H_{\text{PTV}}$  is

$$\begin{aligned} |\Psi_{\text{corr}}^0\rangle = & \mathcal{A} \left( -55.1403\,73 |6s6p^*\rangle - 17.3681\,84 |6s7p^*\rangle + 10.8231\,86 |6s6p\rangle \right. \\ & - 9.5064\,23 |5p^*7s\rangle - 9.2841\,00 |5s6p^*\rangle + 7.8322\,72 |6s8p^*\rangle + 7.1950\,56 |6p^*5d^*\rangle \\ & \left. + 5.5464\,22 |6s9p^*\rangle + 5.5189\,58 |6p5d^*\rangle + 5.1246\,77 |5p^*8s\rangle + \dots \right). \end{aligned}$$

Where  $\mathcal{A} = \sqrt{2} C_T \sigma_N G_F$  and only the first ten important CSFs are listed. The coefficients are much larger than unity but these should be scaled by the parameter  $\sqrt{2} G_F$ . The product of the coupling constant  $C_T$  and nuclear spin  $\sigma_N$  is retained as a parameter and  $C_T$  can be estimated after combining with the experimental results. The above expression for  $|\Psi_{\text{corr}}^0\rangle$  shows that:

1. Like in the lowest order single-particle calculation, the coefficients of the CSFs  $|6snp^*\rangle$  flip sign for  $n \geq 8$ .
2. Most of the important CSFs are singly excited with respect to the ground state CSF  $|6s^2\rangle$ , which is to be expected since  $H_{\text{PTV}}$  is a single particle interaction Hamiltonian.
3. Singly excited configurations like  $|6s6p\rangle$  can contribute through three possible many-body routes. First  $H_{\text{PTV}}$  excites  $|6s^2\rangle$  to  $|6snp^*\rangle$  then a sequence of  $V_{\text{es}}$  connects it to  $|6s6p\rangle$ , second a sequence of  $V_{\text{es}}$  connects  $|6s^2\rangle$  to  $|6p^*6p\rangle$  and  $H_{\text{PTV}}$  takes it to  $|6s6p\rangle$  and third a sequence of  $V_{\text{es}}$  takes  $|6s^2\rangle$  to a CSF  $|\Phi_i\rangle$  which connects to  $|\Phi_j\rangle$  via  $H_{\text{PTV}}$  and another sequence of  $V_{\text{es}}$  connects it to  $|6s6p\rangle$ . Although  $|6s6p\rangle$  cannot connect directly to the ground state  $|6s^2\rangle$  as  $6p$  is close to zero within the nucleus, it is the third most important CSF which contributes to  $|\Psi_{\text{corr}}^0\rangle$ . This demonstrates the importance of many-body effects.
4. The two most important doubly excited odd-parity CSFs for the evaluation of EDM are  $|6p^*5d\rangle$  and  $|6p5d^*\rangle$ . More interesting is the second as both the virtual orbitals involved cannot contribute to the  $H_{\text{PTV}}$  matrix elements. Among the possible many-body routes which can contribute to the co-efficient of  $|6p5d^*\rangle$  one possibility is through the deeper occupied orbitals  $5p^*$  and  $5s$ , which would contribute to core polarization effects.

The value of  $d_a$  is calculated using different sets of CSFs, where the number of either the even or odd CSFs are fixed to the maximum allowed and then increase the number of CSFs in the opposite parity CSF space. The results of such a sequence of calculations is given in the Table III. If the previous sequence of calculation shows the importance of occupied orbitals in the whole CSF space, these two sequences demonstrates the significance of the occupied orbitals in CSF sub-space of each parity.

Like the correlation energy  $\Delta E_0$  there is a significant change of  $d_a$  when CSFs with double excitations from  $6s$  are included. To appreciate the change better the values of  $d_a$  in the two sequence are plotted in Fig.8. Consider the sequence where the number of even-parity CSFs is fixed,  $d_a$  increase with the number of the odd-parity CSFs, which implies that there are no appreciable cancellations due to the odd parity CSFs added. In the second sequence where the number of odd-parity CSFs is fixed,  $d_a$  decreases as the number of even-parity CSFs is increased.

In both the sequence there is a significant change in  $d_a$  when CSFs with double excitation from  $6s$  orbital are added. But, the changes are different in sign, in the even CSF space the inclusion of CSFs with double excitation from  $6s$  increases the value of  $d_a$  where as in the odd-parity CSFs it decreases. Consider the expression for EDM it can be expanded as

$$d_a = 2 \left( \langle \Phi_0 | \vec{D} \Omega_{\text{es,edm}} | \Phi_0 \rangle + \sum_n \langle \Phi_0 | \Omega_{\text{es}}^{\dagger(n)} \vec{D} \Omega_{\text{es,edm}} | \Phi_0 \rangle \right). \quad (6.4)$$

Which can be rewritten in terms of CSF coefficients as

$$d_a = 2 \left[ \langle \Phi_0 | + \sum_i \langle \Phi_i | \mathcal{C}_i^{(\text{es})} \right] \vec{D} \Omega_{\text{es,edm}} | \Phi_0 \rangle = 2 \sum_j \left[ \langle \Phi_0 | + \sum_{i \neq 0} \langle \Phi_i | \mathcal{C}_i^{(\text{es})} \right] \vec{D} \mathcal{C}_j^{(\text{es,edm})} | \Phi_j \rangle. \quad (6.5)$$

Where the definitions of all the quantities are the same as defined in paper-I. Within the whole CSF space, the contribution from the first term is 5.4394 39 and the contribution from the second term is  $-0.6417\ 31$ , which is just 11.80% of the first term. Five most important configurations in the second term from the even-parity sub-space are  $|6p^{*2}\rangle$ ,  $|6p^2\rangle$ ,  $|6p^{*}7p^{*}\rangle$ ,  $|5d^{*2}\rangle$  and  $|6p7p\rangle$  and their contributions are  $-0.8119\ 50$ ,  $0.2065\ 15$ ,  $-0.1001\ 58$ ,  $0.0738\ 55$  and  $0.0599\ 84$  respectively, where  $d_a$  is in units of  $C_T\sigma_N \times 10^{-12}ea_0$ . All these are doubly excited CSFs and mixes with the ground state CSF significantly but the singly excited CSF  $|6s7s\rangle$  which is the third important CSF of  $|\Psi_0\rangle$  does not contribute strongly. In addition there is shift in the sequence of the important CSFs compared to the sequence of contribution to  $|\Psi_0\rangle$ , this is due to difference of dipole and  $H_{\text{PTV}}$  coupling strengths between different CSFs.

Within the whole CSF space considered the value of  $d_a$  is 4.4438 58. In absolute terms this is 0.4804 56 less compared to the lowest order result of 4.9243 136 calculated in an earlier section. A major contribution to this difference is the many-body effects, this is because the direct contributions from the CSFs added to the configuration space is small. Which implies that the contribution from the many-body effects is just 10.81% of the total value and the change is negative. An added advantage of the order by order approach is that the contribution to  $d_a$  can be calculated in terms of the order of residual coulomb interaction. Earlier while calculating the ground state ASF energy it was shown how a truncation in the order of  $V_{\text{es}}$  perturbation can give an inaccurate value of  $E_0$ .

## B. Cluster Based Formulations

The CEPA-0 wave-operator equations of  $\Omega_{\text{es}}$  and  $\Omega_{\text{es},\text{edm}}$  are identical to the linearized coupled-cluster equations. The atomic Yb EDM  $d_a$  calculated using CEPA-0 using the same sequence of CSFs as in Table III are given in Table IV and the following can be inferred:

1. The results from CEPA-0 do not differ significantly from the MBPT results for the singly excited CSFs with core configurations  $|6s\rangle$  and  $|4f^{13}6s^2\rangle$ . This is because the non-linear terms do not contribute since the configuration space is spanned by singly excited CSFs.
2. A significant difference from the MBPT results is expected when doubly excited CSFs are included in the CSF space. This is observed when the CSFs having core configuration  $|4f^{13}6s^1\rangle$  are included. The change of  $d_a$  calculated using MBPT by fixing the number of odd parity CSFs to 17087 is  $-0.5599\ 84$ , whereas CEPA-0 reduces the change to  $-0.1091\ 50$ .
3. Within the whole CSF space considered, the value of  $d_a$  calculated using CEPA-0 is 5.9421 36, which is 25.21% larger than the MBPT result. The difference gives a rough estimate of the contribution from the non-linear terms in the cluster equation. It is a rough estimate as the MBPT calculation also includes the contribution from the size-inconsistent terms, which are unphysical and are not included in the CEPA formalism.

The CEPA-0 calculation does not include size-consistent non-linear terms of  $\Omega_{\text{es}}$  and  $\Omega_{\text{es},\text{edm}}$ . The results using the CEPA-2 equations are tabulated in Table V. To make comparisons convenient the calculation is done with the same choice of CSF sequence as before. Comparing with the results from the calculations using MBPT and CEPA-0 give the following:

1. The calculation within the CSF space of singly excited even parity CSFs with core configurations  $|6s\rangle$  and  $|4f^{13}6s\rangle$  and all the odd parity CSFs is identical with the result calculated using CEPA-0. This implies that the contribution from the non-linear EPV terms with  $T_{\text{es}}(1)$  from the even parity subspace is negligible. But, it is different from the MBPT result of the same CSF space. And the difference of 0.2067 67 is due to the EPO non-linear terms, which are included in the MBPT.
2. Consider the calculation within the CSF space consisting of all the even parity CSFs and the singly excited odd parity CSFs having core configurations  $|6s\rangle$  and  $|4f^{13}6s\rangle$ . The CEPA-2 and MBPT results differ by less than 2%. But, the result from CEPA-0 differs from both by more than 12%. This shows that the contribution from non-linear terms with  $T_{\text{PTV}}(1)$  is not negligible or the contribution from the size-consistent is significant, with the present results it is difficult to distinguish between the two.
3. The  $d_a$  calculated within the whole CSF space considered is 4.5065 25 and is larger than the MBPT result by 1.4% and less than the CEPA-0 result by 31.86%. This implies that the contribution of non-linear terms to  $d_a$  is very important.

The effect of the EPO unlinked terms in  $\Omega_{\text{es},\text{edm}}$  can be estimated by calculating  $T_{\text{es},\text{edm}}$  with the EPO renormalization terms included. The results are given in Table VI. The final value with the full CSF space is 4.2446 91, which

is suppressed by 5.8% compared to the CEPA-2 result. This difference is due to the EPO contribution to the renormalization term in  $\Omega_{\text{es,edm}}$ . Another property which can be compared to gain an insight on the contribution of the size-inconsistent terms is the energy of the ground state  $E_0$ . The value of  $E_0$  calculated using the wave-operator  $\Omega_{\text{es}}$  derived here has no contribution from the size inconsistent terms but it excludes some of the less important size-consistent terms. The difference in the value  $E_0$  calculated using the Bloch-equation and  $\Omega_{\text{es}}$  derived from the cluster equation gives the contribution from the size inconsistent terms. Like in  $d_a$  the approximation is that the contribution from the EPO size consistent terms non-linear in cluster amplitudes is very small, then the difference in the result can in principle be accounted to the size inconsistent terms.

## VII. CONCLUSION

Comparing the results from different methods, it is clear that a size-consistent theory is preferable for high accuracy computation of atomic EDM and the contribution from the non-linear terms in the cluster amplitude is also important. With the present calculation the difference between the MBPT and CEPA-2 result cannot be accounted distinctly to non-linear terms or the size-inconsistent terms. A better comparison can be made after including all the non-linear terms in the cluster amplitudes. As the orbital space is made larger, the size of the CSF space grows very large. This puts a limitation during the calculation as the memory requirement increases, it is manageable if the calculation is done at the level of single particle-Moller-Plesset partitioning of the atomic Hamiltonian. At the single particle level the cluster equation with the residual coulomb interaction Hamiltonian reduces to the method used by Blundell [20] and his collaborators. The inclusion of terms non-linear in cluster amplitudes is also relatively easy as compared to the EN-partitioning. To check the quality of the wave functions, experimentally known quantities like hyperfine constants and excitation energies needs to be calculated. These will be reported in our later papers.

## VIII. ACKNOWLEDGMENTS

We thank our colleagues Rajat Choudury, Holger Merlitz and P. Panda for many useful discussions we had and the computer staff for making available to us the r10000 power challenge.

- 
- [1] T. G. Vold, F. J. Raab, H. Heckel and E. N. Fortson, Phys. Rev. Lett. **52**, 2229(1984).
  - [2] M. V. Romalis, W C Griffith and J. P. Jacobs and E. N. Fortson, Phys. Rev. Lett. **86**, 2505 (2001)
  - [3] E. Eliav, U. Kaldor, and Y. Ishikawa, Phys. Rev. A **52**, 291-296 (1995).
  - [4] S. Porsev, Yu. G. Rakhlin and M. G. Kozlov, J. Phys. B. **32**, 1113(1999).
  - [5] S. G. Porsev, Yu. G. Rakhlin and M. G. Kozlov, Phys. Rev. A **60**, 2781(1999).
  - [6] J. Migdalek and W. E. Baylis Phys. Rev. A **33**, 1417-1420 (1986)
  - [7] C. J. Bowers, D. Budker, E. D. Commins, D. DeMille, S. J. Freedman, A.-T. Nguyen, S.-Q. Shang, and M. Zolotarev Phys. Rev. A **53**, 3103-3109 (1996).
  - [8] M. Watanabe, R. Ohmukai, U. Tanaka, K. Hayasaka, H. Imajo and S. Urabi, JOSA B **13**, 2377,(1996).
  - [9] K. Honda, Y. Takahashi, T. Kuwamoto, M. Fujimoto, K. Toyoda, K. Ishikawa, and T. Yabuzaki, Phys. Rev. A **59**, R934-R937,(1999).
  - [10] Y. Takahashi, M. Fujimoto, T. Yabuzaki, Angom Dilip Singh, Manoj K. Samal and B. P. Das, in Proceedings of CP Violation and its Origin, edited by K. Hagiwara(KEK Reports, Tsukuba, 1997).
  - [11] M. V. Romalis and E. N. Fortson, Phys. Rev. A **59**, 4547(1999).
  - [12] S. M. Barr, Int. J. Mod. Phys. A **8**,209,(1993).
  - [13] V. V. Flambaum and J. S. M. Ginges, arXiv:nucl-th/0108007
  - [14] Angom Dilip, Bhanu Pratap Das, Warren F Perger, M K Samal and K P Geetha, Jour. Phys. B **34**, 3089(2001).
  - [15] Ingvar Lindgren and John Morrison, *Atomic Many-Body Theory*(Springer, New York, 1982).
  - [16] J. Goldstone, Proc. Roy. Soc.(London) **A239**, 267(1957).
  - [17] C. Bloch, Nucl. Phys. **6**, 329(1958).
  - [18] L. M. Frantz and R. L. Mills **15**, 16(1960).
  - [19] W. Kutzelnigg, Methods in Electronic Structure Theory, Ed by H. F. Schaefer (Plenum, New York, 1977).
  - [20] S. A. Blundell, W. R. Johnson and J. Sapirstein, Phys. Rev. A **43**, 3407(1991).

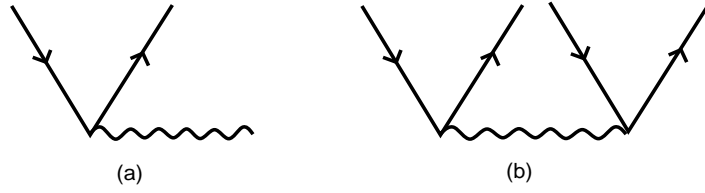


FIG. 1. Diagrams for the wave-operators (a)  $\Omega_{\text{es}}(1)$  and (b)  $\Omega_{\text{es}}(2)$ .

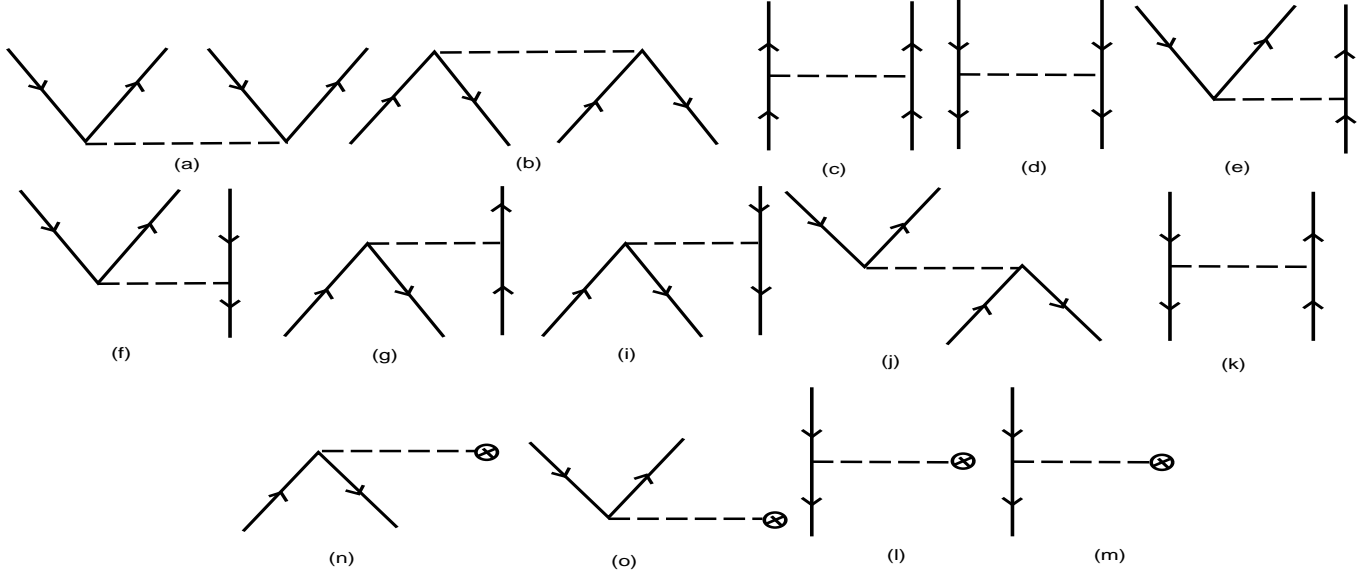


FIG. 2. The diagrams for the residual Coulomb interaction  $V_{\text{es}}$ .

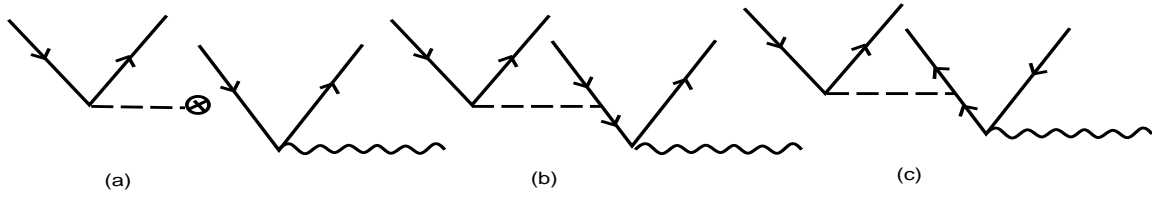


FIG. 3. The diagrammatic representations of the term  $\langle \Phi_{ab}^{rs} | V_{\text{es}} | \Phi_{a'}^{r'} \rangle x_{a'}^{r'}$ .

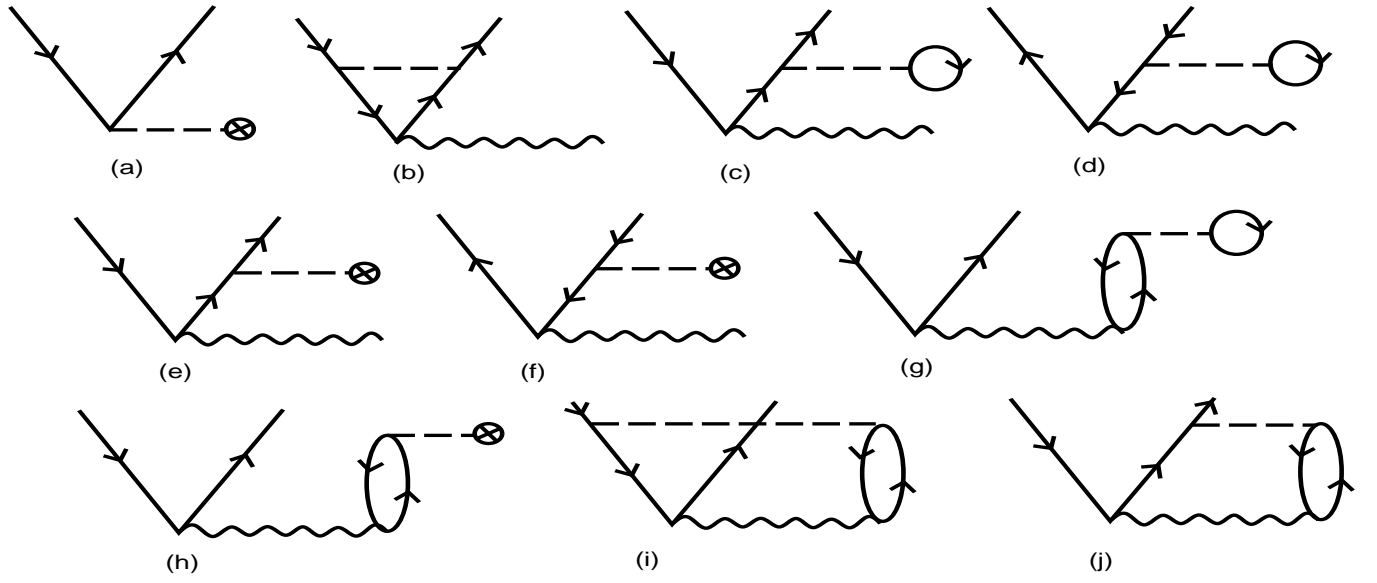


FIG. 4. Diagrams that contribute to the single-excitation cluster amplitude.

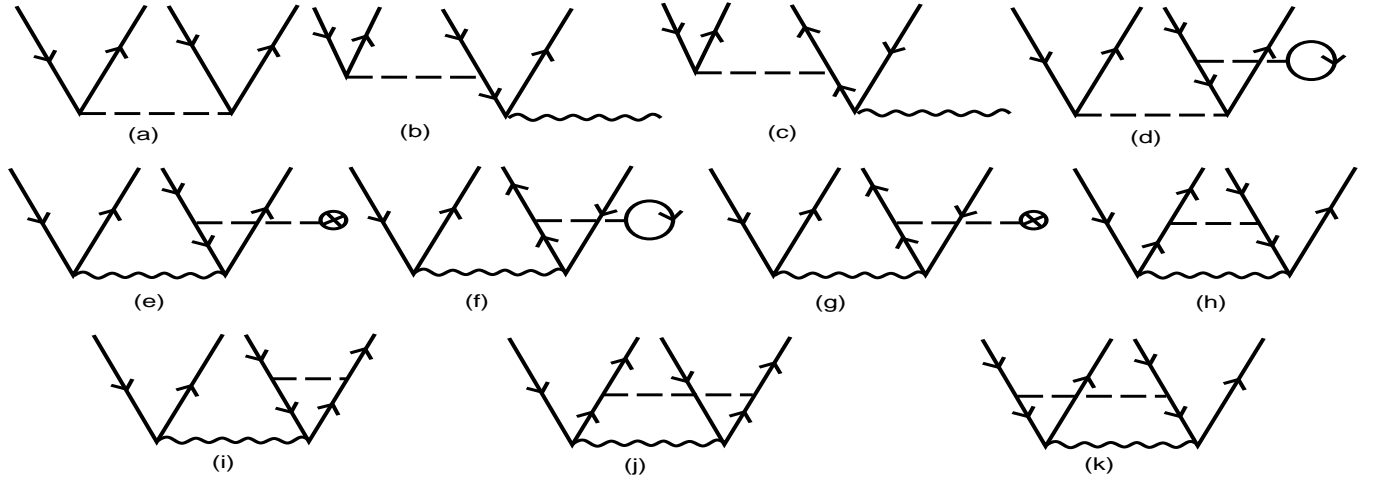
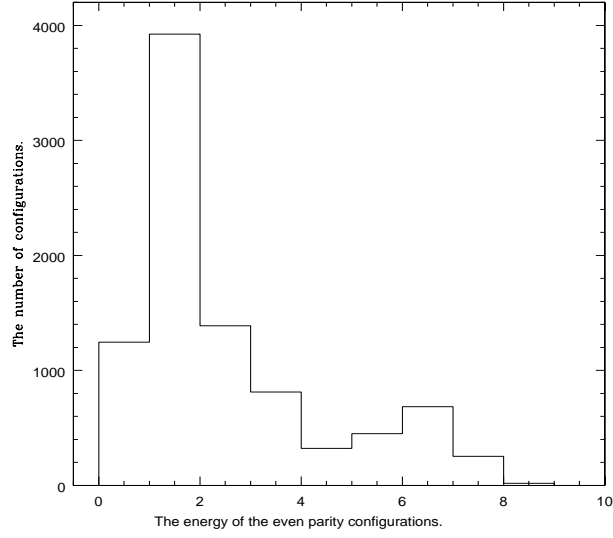
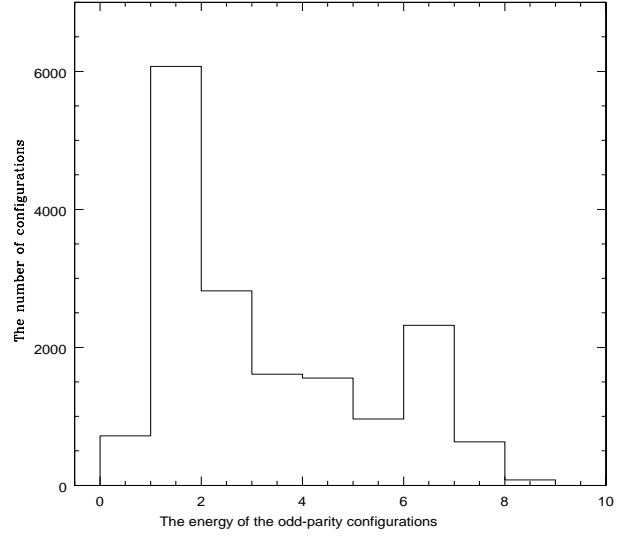


FIG. 5. The diagrams for the terms in doubly-excited cluster operator equation.

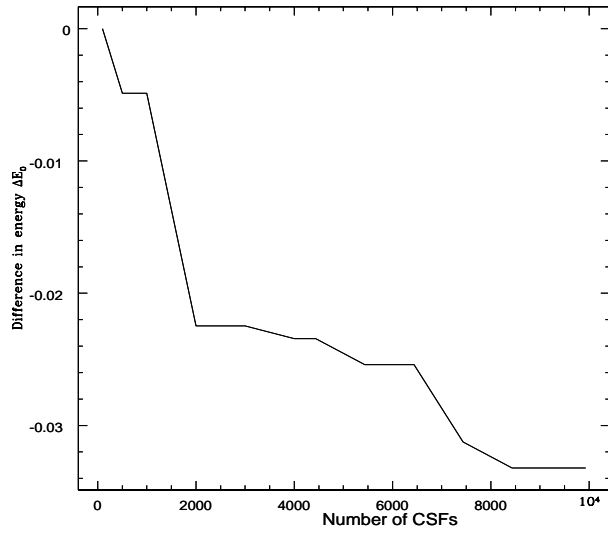


(a)

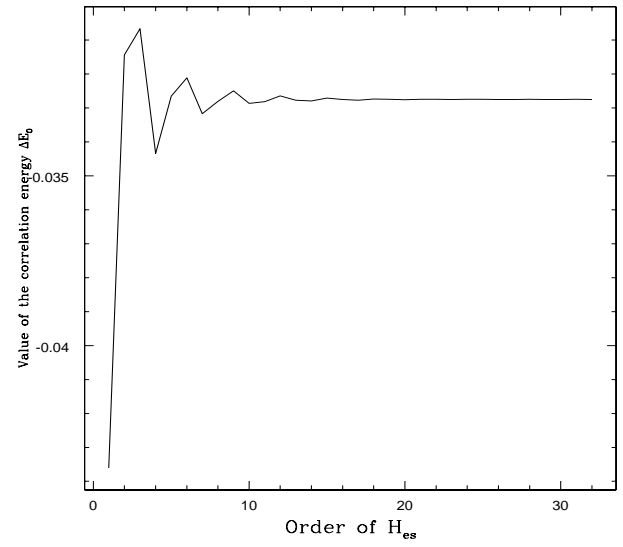


(b)

FIG. 6. Histogram of  $|E|$  for the even parity CSFs.



(a)



(b)

FIG. 7. The change in energy due to many-body effects introduced by the configurations.



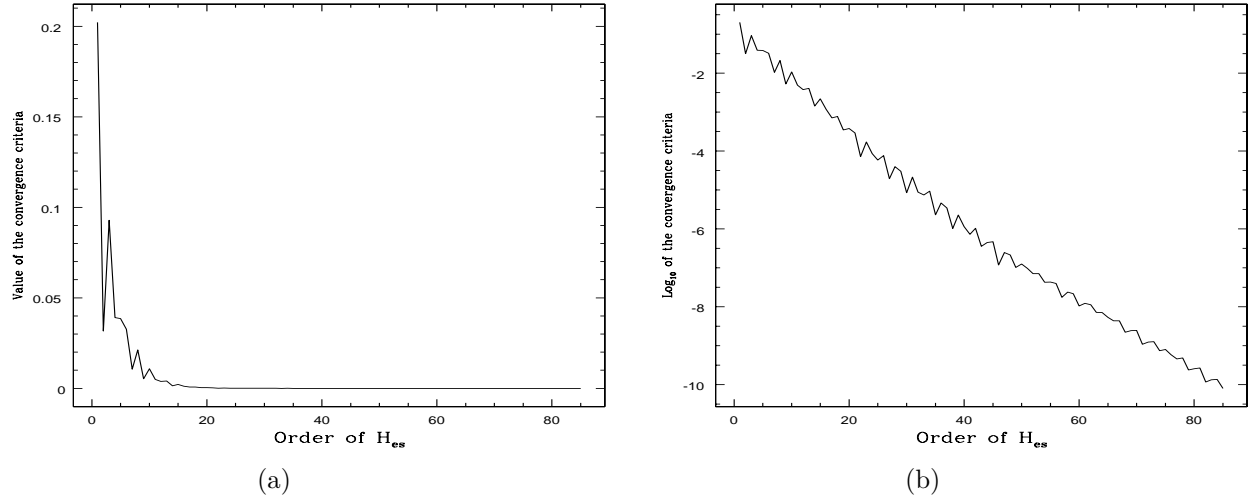


FIG. 8. The convergence of the wave-operators

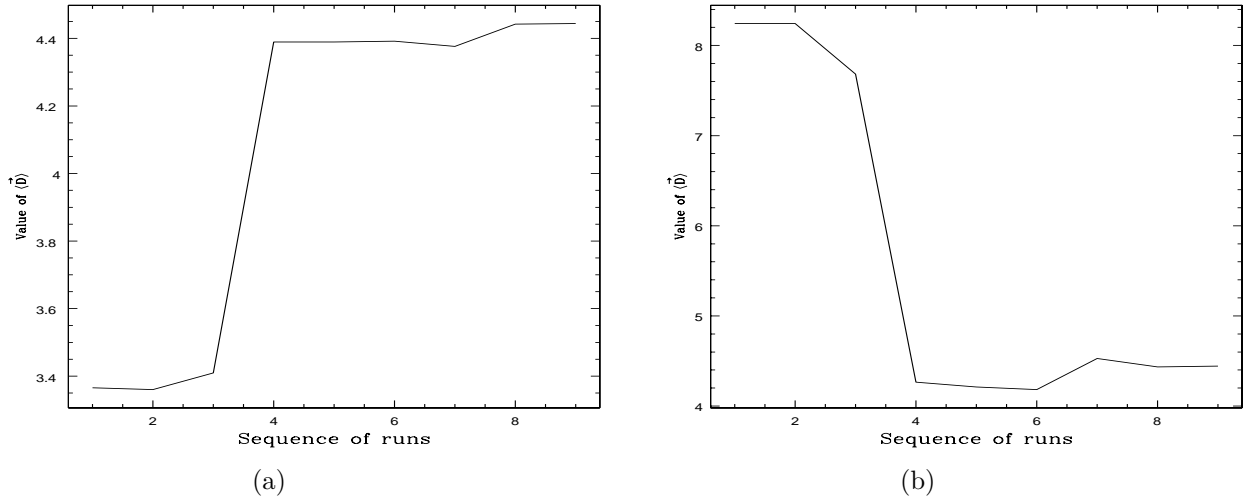


FIG. 9. The value of  $d_a$

TABLE I. The number of the CSFs with different occupied configurations.

Sl.no	Occupied part	Configurations		Sl.no	Occupied part	Configurations	
		Even	Odd			Even	Odd
1	$ 6s\rangle$	6	12	2	$ 4f^{14}\rangle$	147	287
3	$ 4f^{13}6s^2\rangle$	12	18	4	$ 4f^{13}6s^1\rangle$	1224	3618
5	$ 4f^{12}6s^2\rangle$	3045	7739	6	$ 5p^5 4f^{14} 6s^2\rangle$	12	30
7	$ 5p^5 4f^{14} 6s^1\rangle$	1044	1668	8	$ 5p^5 4f^{13} 6s^2\rangle$	3604	2394

TABLE II. The energy of the ground state ASF with increasing CSF-space size.

Sl. no	No of CSF	Energy	Sl. no	No of CSF	Energy
1	100	-14067.6714 79	2	500	-14067.6755 69
3	1000	-14067.6756 60	3	2000	-14067.6942 64
5	3000	-14067.6942 68	6	4000	-14067.6949 91
7	4435	-14067.6949 91	8	5435	-14067.6974 13
9	6435	-14067.6974 21	10	7435	-14067.7019 28
11	8435	-14067.7040 97	12	9094	-14067.7040 97
13	9594	-14067.7042 26	14	9930	-14067.7042 26

TABLE III. Values of  $d_a$  for different number of even and odd parity configurations.

Sl. no	No of CSFs		$d_a$	Sl. no	No of CSFs		$d_a$
	Even	Odd			Even	Odd	
1	9930	12	3.3654 83	10	7	17087	8.2430 89
2	9930	30	3.3605 54	11	19	17087	8.2430 89
3	9930	3648	3.4095 46	12	1243	17087	7.6831 05
4	9930	3846	4.3895 21	13	1390	17087	4.2645 44
5	9930	11676	4.3895 43	14	4435	17087	4.2118 95
6	9930	14070	4.3916 11	15	4448	17087	4.1837 51
7	9930	14100	4.3760 30	16	6713	17087	4.5282 75
8	9930	15768	4.4424 65	17	9094	17087	4.4333 81
9	9930	17087	4.4438 58	18			

TABLE IV. Value of  $d_a$  computed using the CEPA-0 formalism.

Sl. no	No of CSFs		$d_a$	Sl. no	No of CSFs		$d_a$
	Even	Odd			Even	Odd	
1	9930	12	3.8250 23	10	7	17087	8.4499 64
2	9930	30	3.8426 96	11	19	17087	8.4499 64
3	9930	3648	3.9252 41	12	1243	17087	8.3408 14
4	9930	3846	5.7783 09	13	1390	17087	5.5126 26
5	9930	11676	5.7783 88	14	4435	17087	5.5091 16
6	9930	14070	5.7820 42	15	4448	17087	5.3769 11
7	9930	14100	5.8370 85	16	6713	17087	5.6132 71
8	9930	15768	5.9437 56	17	9094	17087	5.9275 26
9	9930	17087	5.9421 36				

TABLE V. Table V: Values of  $d_a$  computed with CEPA-2.

Sl. no	No of CSFs		$d_a$	Sl. no	No of CSFs		$d_a$
	Even	Odd			Even	Odd	
1	9930	12	3.3130 75	10	7	17087	8.4499 64
2	9930	30	3.3133 86	11	19	17087	8.4499 64
3	9930	3648	3.3684 39	12	1243	17087	7.8528 23
4	9930	3846	4.4589 69	13	1390	17087	4.3791 81
5	9930	11676	4.4589 33	14	4435	17087	4.3758 71
6	9930	14070	4.4608 15	15	4448	17087	4.3558 36
7	9930	14100	4.4581 78	16	6713	17087	4.4547 38
8	9930	15768	4.5149 07	17	9094	17087	4.4981 25
9	9930	17087	4.5065 25				

TABLE VI. Values of  $d_a$  computed with the EPO components included in the cluster amplitudes  $\overline{\mathcal{T}}$ .

Sl. no	No of CSFs		$d_a$	Sl. no	No of CSFs		$d_a$
	Even	Odd			Even	Odd	
1	9930	12	3.1704 91	10	7	17087	8.4499 64
2	9930	30	3.1682 67	11	19	17087	8.4499 64
3	9930	3648	3.2196 53	12	1243	17087	7.8521 84
4	9930	3846	4.2130 96	13	1390	17087	4.3783 45
5	9930	11676	4.2130 54	14	4435	17087	4.3042 71
6	9930	14070	4.2147 05	15	4448	17087	4.2332 39
7	9930	14100	4.2039 41	16	6713	17087	4.2802 30
8	9930	15768	4.2539 59	17	9094	17087	4.2375 23
9	9930	17087	4.2446 91	18			